4

Magnetotelluric Tensor Decomposition: Insights from Linear Algebra and Mohr Diagrams

F.E.M.(Ted) Lilley
Research School of Earth Sciences, Australian National University, Canberra Australia

1. Introduction

The magnetotelluric (MT) method of geophysics exploits the phenomenon of natural electromagnetic induction which takes place at and near the surface of Earth. The purpose is to determine information about the electrical conductivity structure of Earth, upon which the process of electromagnetic induction depends. The MT method has been well described recently in books such as Simpson & Bahr (2005), Gubbins & Herrero-Bervera (2007), and Berdichevsky & Dmitriev (2008). The reader is referred to these for general information about the method and its results. Notable modern extensions of the method are observation at an array of sites simultaneously, and observation on the seafloor (both shallow and deep oceans).

In the most simple form of the method, data are observed at a single field site. Typically, three components (north, east and vertically downwards) of the fluctuating magnetic field are observed, and two components (north and east) of the fluctuating electric field. The magnetic field is measured using a variety of instruments such as fluxgates and induction coils. The electric field is measured more simply, between grounded electrodes typically several hundred metres apart.

The natural signals observed cover a frequency band from 0.001 to 1000 Hz. They have a variety of causes, the relative importance of which varies with position on the Earth, especially latitude. Recorded data are transformed to the frequency domain, and interpretation proceeds based on frequency-dependence.

The reduction of observed time-series to the frequency domain is thus fundamental to the MT method. In the frequency domain various transfer functions are determined, encapsulating the response of the observing site to the source fields causing the induction.

Another fundamental part of the data-reduction process, the focus of the present chapter, is "rotation" of observed data. By rotation is meant an examination of the observed transfer functions to see how they would vary were the observing axes rotated at the observing site. Rotation may reveal geologic dimensionality, and strike direction.

The MT tensor has a 2 x 2 form and is well-suited to analysis by the methods of linear algebra. This suitability was evident early in the development of MT, and it is common for a paper on MT to start with such an analysis. The papers of Eggers (1982), LaTorraca et al. (1986), and Yee & Paulson (1987), for example, specifically proceed with eigenvalue analysis and singular value decomposition (SVD), and see also Weaver (1994).

There appear however to be a number of aspects of this approach as yet unexplored, especially when the in-phase and quadrature parts of the tensor are analysed separately. This chapter now follows such a line of enquiry, investigating the significance of symmetric, antisymmetric and non-symmetric parts, eigenvalue analysis and SVD.

The Mohr diagram representation is found to be a useful way to display some of the results. Cases of 1D, 2D and 3D electrical conductivity structure are examined, including the 3D case where the MT phase is greater than 90° or "out of quadrant".

Taking the Smith (1995) treatment of telluric distortion, a particular case examined is that where SVD gives an angle which is frequency independent, implying that it contains geological information. Such angles arise when MT tensor data are nearly singular.

The analysis of in-phase and quadrature parts separately is seen to give further insight into the question of whether, as suspected by Lilley (1998), the determinants of the parts taken separately should always be positive.

2. Notation

The common representation of a magnetotelluric tensor $\mathbf{Z}$ is taken,

$$\mathbf{E} = \mathbf{Z}\mathbf{H} \tag{1}$$

of components

$$\begin{bmatrix} E_x \\ E_y \end{bmatrix} = \begin{bmatrix} Z_{xx} & Z_{xy} \\ Z_{yx} & Z_{yy} \end{bmatrix} \begin{bmatrix} H_x \\ H_y \end{bmatrix} \tag{2}$$

linking observed electric $\mathbf{E}$ and magnetic $\mathbf{H}$ fluctuations at an observing site on the surface of Earth.

All quantities are complex functions of frequency ω, and in Equations 1 and 2 a time dependence of $\exp(i\omega t)$ is understood.

In this chapter the subscripts p, q will be used to denote in-phase and quadrature parts. For example the complex quantity Z^σ is expressed

$$Z^\sigma = Z_p^\sigma + iZ_q^\sigma \tag{3}$$

Note that adopting a time-dependence of $\exp(-i\omega t)$ as recommended by authors such as Stratton (1941) and Hobbs (1992) would change the sign of Z_q^σ. Such a change may be misinterpreted, especially when distortion has caused the phase to be out of its expected first quadrant.

The subscripts p, q will also be used to denote quantities which are derived from the in-phase and quadrature parts, respectively, of a complex quantity, but which are themselves not recombined to give a further complex quantity. In Sections 2.1, 3, 5 and 11 below, where derivations apply equally to in-phase and quadrature cases, subscripts p, q are omitted for simplicity. Such derivations can be taken as applying to in-phase components, with similar derivations possible for quadrature components.

Also in this chapter, for compactness of text, a 2 x 2 matrix such as that for $\mathbf{Z}$ in Equation 2 will in places be written $[Z_{xx}, Z_{xy}; Z_{yx}, Z_{yy}]$. A rotation matrix $\mathbf{R}(\theta)$ will be introduced

$$\mathbf{R}(\theta) = [\cos\theta, \sin\theta; -\sin\theta, \cos\theta] \tag{4}$$

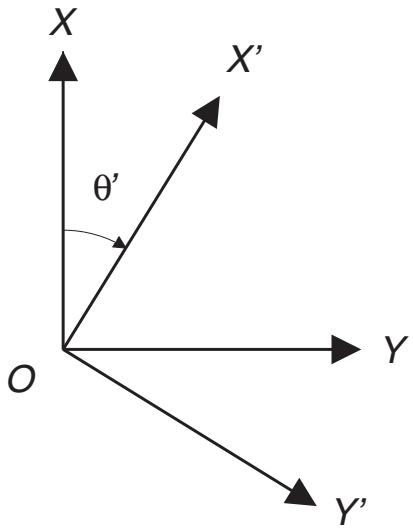

Fig. 1. The rotation of MT observing axes clockwise by angle θ', from OX and OY (north and east) to OX′ and OY′.

with $\mathbf{R^T}(\theta)$ the transpose of $\mathbf{R}(\theta)$. $\mathbf{R^T}(\theta)$ will sometimes be written $\mathbf{R}(-\theta)$.

2.1 Rotation of the horizontal axes

Upon rotation of the horizontal measuring axes clockwise by angle θ' as shown in Fig. 1, matrix $[Z_{xx}, Z_{xy}; Z_{yx}, Z_{yy}]$ changes to $[Z'_{xx}, Z'_{xy}; Z'_{yx}, Z'_{yy}]$ according to

$$\begin{bmatrix} Z'_{xx} & Z'_{xy} \\ Z'_{yx} & Z'_{yy} \end{bmatrix} = \mathbf{R}(\theta') \begin{bmatrix} Z_{xx} & Z_{xy} \\ Z_{yx} & Z_{yy} \end{bmatrix} \mathbf{R}(-\theta') \tag{5}$$

Thus the elements of the second matrix are related to the first by the following equations:

$$Z'_{xx} = (Z_{xx} + Z_{yy})/2 + C\sin(2\theta' + \beta) \tag{6}$$

$$Z'_{xy} = (Z_{xy} - Z_{yx})/2 + C\cos(2\theta' + \beta) \tag{7}$$

$$Z'_{yx} = -(Z_{xy} - Z_{yx})/2 + C\cos(2\theta' + \beta) \tag{8}$$

$$Z'_{yy} = (Z_{xx} + Z_{yy})/2 - C\sin(2\theta' + \beta) \tag{9}$$

where

$$C = [(Z_{xx} - Z_{yy})^2 + (Z_{xy} + Z_{yx})^2]^{\frac{1}{2}}/2 \tag{10}$$

and β is defined by

$$\tan\beta = (Z_{xx} - Z_{yy})/(Z_{xy} + Z_{yx}) \tag{11}$$

It is also useful to define an auxiliary angle β' by

$$\tan \beta' = (Z'_{xx} - Z'_{yy})/(Z'_{xy} + Z'_{yx}) \tag{12}$$

with

$$\theta' = (\beta' - \beta)/2 \tag{13}$$

and angle μ as

$$\tan \mu = (Z_{yy} + Z_{xx})/(Z_{xy} - Z_{yx}) \tag{14}$$

also Z^L as

$$Z^L = [(Z_{xx} + Z_{yy})^2 + (Z_{xy} - Z_{yx})^2]^{\frac{1}{2}}/2 \tag{15}$$

Then plotting Z'_{xx} against Z'_{xy} as the axes are rotated (i.e. θ' varies) defines a circle, known (with its axes) as a Mohr diagram. On such a figure axes for Z'_{yx} and Z'_{yy} may be included, to display the variation of these components also.

3. The depiction of MT tensors using Mohr diagrams

The Mohr diagram representation, straightforward for a 2 x 2 matrix, is an informative figure for the student of linear algebra. For the MT case it may be a useful way to display results, as will now be shown for the general case of 3D conductivity structure, and the particular cases of 2D and 1D conductivity structure to which the 3D case simplifies.

In this chapter in-phase and quadrature data will be presented in adjacent figures. There is an appeal in putting both in-phase and quadrature data on the same axes, as demonstrated by Szarka & Menvielle (1997) and Weaver et al. (2000), but when showing a full frequency range separate sets of axes are practical. Also at times it is helpful to add axes for Z'_{yx} and Z'_{yy} as on Fig. 2a, and such an addition is not possible for Z'_{xx} and Z'_{xy} axes common to both in-phase and quadrature parts.

3.1 The general case; 3D structure

Mohr diagrams for the general case of the MT tensor are shown in Fig. 2a. Different points on the diagram can be checked to confirm that Equations 6 to 15 for the rotation of axes are obeyed. The diagram is "Type 1" of Lilley (1998, p.1889), and shows how axes for Z'_{yx} and Z'_{yy} can be included. The diagram in Fig. 2a is drawn for relatively mild 3D characteristics. Diagrams for strong 3D characteristics are discussed below and shown in an example; however, what limits there may be to extreme 3D behaviour have not yet been fully explored. Some examples of 3D behaviour which appear to be prohibited will be discussed in this chapter.

3.2 2D structure

When the geologic structure is 2D and the axes are rotated to be along and across geologic strike, the MT tensor can be rotated to have the form $[0, Z^\sigma; -Z^\chi, 0]$, where it is expected both Z^σ and Z^χ are positive (a point discussed in Section 13.1 below). As shown in Fig. 2b, the diagram becomes a pair of circles with origins on the Z'_{xy} axes, and angles μ_p and μ_q are zero. The in-phase and quadrature radial arms are parallel. Z^σ and Z^χ are known as the TE and TM modes (or vice-versa).

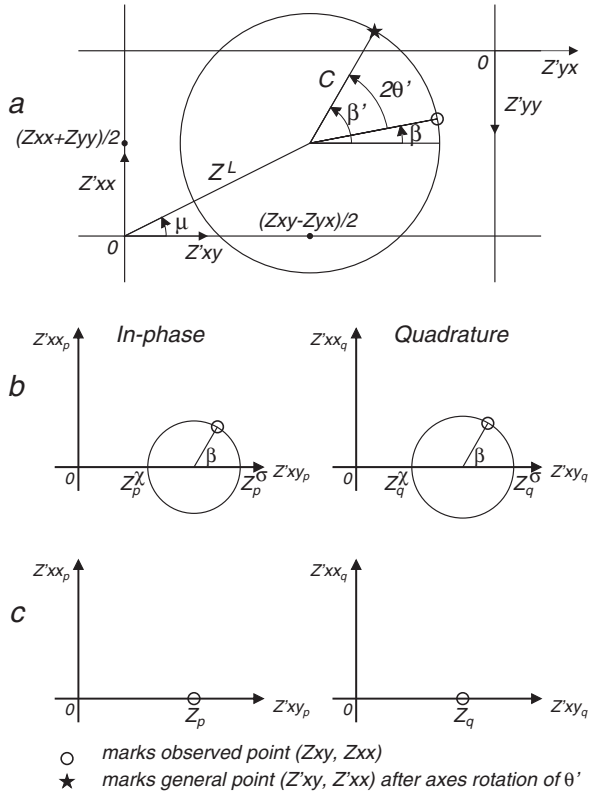

Fig. 2. Mohr diagrams for a: The general MT tensor; both in-phase and quadrature parts take this general form. b: The 2D case; radial arms are now parallel, with circle centres on the horizontal axes. The 2D values Z^{σ} and Z^{χ} could be interchanged. c: The 1D case, for **Z** observed as $[0, Z; -Z, 0]$.

3.3 1D structure

If a 2D case simplifies further to become a 1D case, $Z^{\sigma} = Z^{\chi} = Z$ say, and the tensor for all rotations has the form $[0, Z; -Z, 0]$. The length C of the radial arm vanishes, and the diagram reduces to a pair of points on the horizontal axes, as shown in Fig. 2c.

4. Invariants of rotation of the measuring axes

It can be seen from Fig. 2a that the MT observations can be expressed in terms of seven invariants of rotation. From different sets which are possible, and evident from formal analysis (Szarka & Menvielle, 1997; Weaver et al., 2000), this chapter adopts the invariants shown in Fig. 3. Thus the eight values of the MT tensor, all of which generally change upon axes rotation, become seven invariants plus one angle. That angle, θ' in Fig. 2a, is the angle which defines the direction of the measuring axes (for example, with respect to north).

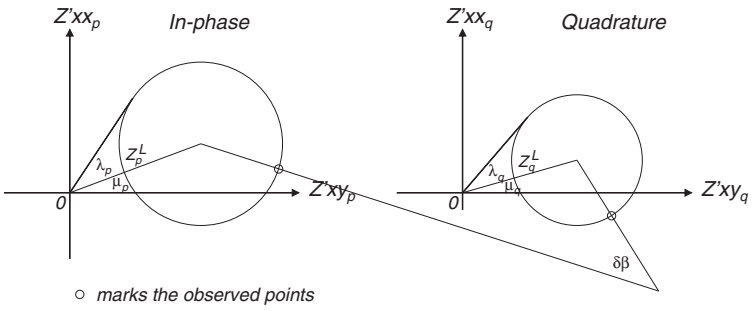

Fig. 3. Seven invariants of rotation for a general 3D MT tensor.

4.1 Two invariants summarising the 1D character of the tensor

The two invariants $Z^L_{p,q}$ summarising the 1D character are straightforward and were termed "central impedances" by Lilley (1993). Note that the second could be expressed normalised by the first, and so as a ratio (and then as an angle, taking the arctangent of that ratio).

4.2 Two invariants summarising the 2D character of the tensor

Two invariants $\lambda_{p,q}$ measure the 2D character, and are also straightforward. They are naturally angles, and were termed anisotropy angles by Lilley (1993). They may be expressed

$$\lambda_{p,q} = \arcsin(C_{p,q}/Z^L_{p,q}) \tag{16}$$

where $\lambda_{p,q}$ is in the range 0 to 90°. (Note this definition fails if $C_{p,q} > Z^L_{p,q}$ and the relevant circle encloses the origin.)

4.3 Two (of three) invariants summarising the 3D character of the tensor

Two angles $\mu_{p,q}$ characterising the 3D nature of the impedance tensor are also straightforward, and are shown in Fig. 3. It may be effective to express them as their mean and difference values, because certain mechanisms for causing 3D effects, especially static distortion, give the same μ contribution to both the in-phase and quadrature parts of a tensor (Lilley, 1993). In such cases, static distortion of a regional 2D structure is then measured by $(\mu_q + \mu_p)/2$, and the difference $(\mu_q - \mu_p)$ would be zero. Thus $(\mu_q - \mu_p)$, when non-zero, may be a measure of any 3D effects present, beyond static distortion.

4.4 The third 3D invariant

A third 3D invariant $(\delta\beta = \beta_q - \beta_p)$ can be seen from Fig. 3 to be the angle by which the two radial arms of the in-phase and quadrature circles are not parallel. It is significant as it alone, of the invariants chosen, links the in-phase and quadrature parts of an observed tensor. Another possibility for this seventh invariant is $(\delta\beta - \mu_q + \mu_p)$, where the difference $(\mu_q - \mu_p)$ is removed first from $\delta\beta$, and the departure of the radial arms from being parallel is then judged afresh.

However a related angle for the seventh invariant, derived by Weaver et al. (2000), has the great utility that it appears again in the Mohr diagram for the phase tensor, to be introduced in Section 8 below. There, as angle γ, it has a simple significance concerning geologic strike.

4.5 Angles or their sines?

Weaver et al. (2000) take sines of the angles to give measures in the range 0 to 1, and this technique is adopted by Marti et al. (2005). However, if ambiguity is to be avoided, such a procedure restricts the angles to being not greater than 90°. Because examples occur for which the values of $\mu_{p,q}$ are greater than 90°, it may be preferable to quote the invariants as angles, allowing them a 360° range (perhaps most usefully expressed in the range ±180°).

5. Some basic techniques of linear algebra applied to the analysis of the MT tensor

To gain familiarity with the MT tensor, it is instructive to explore some common steps taken in matrix analysis. The steps described form part of the history of MT.

5.1 Separation into symmetric and antisymmetric components

The MT tensor $\mathbf{Z}$, if split into symmetric $\mathbf{Z^s}$ and antisymmetric $\mathbf{Z^a}$ parts

$$\mathbf{Z} = \mathbf{Z^s} + \mathbf{Z^a} \tag{17}$$

may be written

$$\begin{bmatrix} Z_{xx} & Z_{xy} \\ Z_{yx} & Z_{yy} \end{bmatrix} = \begin{bmatrix} Z_{xx} & (Z_{xy}+Z_{yx})/2 \\ (Z_{xy}+Z_{yx})/2 & Z_{yy} \end{bmatrix} + \begin{bmatrix} 0 & (Z_{xy}-Z_{yx})/2 \\ (Z_{yx}-Z_{xy})/2 & 0 \end{bmatrix} \tag{18}$$

The second and antisymmetric part, $\mathbf{Z^a}$, is immediately recognised as being of the ideal 1D MT form described in Section 3.3.

In much MT interpretation, it has been common practice to obtain "1D estimates" from 2D or 3D data by taking the average of observed Z_{xy} and $(-)Z_{yx}$ as $(Z_{xy} - Z_{yx})/2$. Equation 18 demonstrates the approximations made in such a procedure. For in taking such an average, it can be seen that the information in the first matrix term $\mathbf{Z^s}$ is ignored, perhaps without justification. Diagrammatically, the procedure is equivalent, in Fig. 4a, to representing the circle on the left-hand side by the sum of the two circles on the right-hand side. The first circle on the right-hand side is then ignored, leaving the second circle which, reduced to its central point, is a 1D case.

5.2 Separation into symmetric and 2D components

The exercise in Section 5.1 may be regarded as a separation into symmetric and 1D components, and suggests a similar separation of the observed tensor into two parts of which the second, $\mathbf{Z^{2D}}$, is chosen to be of ideal 2D form. The first part, $\mathbf{Z^{s2}}$, is found to again be symmetric.

Thus the MT tensor is expressed

$$\mathbf{Z} = \mathbf{Z^{s2}} + \mathbf{Z^{2D}} \tag{19}$$

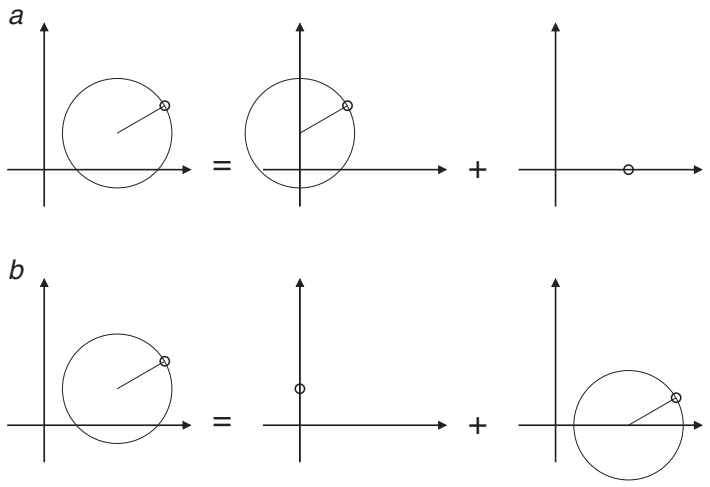

Fig. 4. Separation of a 2 x 2 matrix, a: into symmetric and 1D parts as in Equation 18; b: into symmetric and 2D parts as in Equation 20. The diagrams are drawn for $\mathbf{Z} = [1.75, 3.30; -0.70, 0.25]$. Thus case a is: $\mathbf{Z} = [1.75, 1.3; 1.3, 0.25] + [0, 2.0; -2.0, 0]$, and case b is: $\mathbf{Z} = [1.0, 0; 0, 1.0] + [0.75, 3.3; -0.7, -0.75]$.

and by partition as

$$\begin{bmatrix} Z_{xx} & Z_{xy} \\ Z_{yx} & Z_{yy} \end{bmatrix} = \begin{bmatrix} (Z_{xx} + Z_{yy})/2 & 0 \\ 0 & (Z_{xx} + Z_{yy})/2 \end{bmatrix} + \begin{bmatrix} (Z_{xx} - Z_{yy})/2 & Z_{xy} \\ Z_{yx} & (-Z_{xx} + Z_{yy})/2 \end{bmatrix} \quad (20)$$

where the second part is now of ideal 2D form.

Equation 20 is expressed in Mohr diagrams in Fig. 4b, where it can be seen that the first part is a point on the vertical axis, and the second part, $\mathbf{Z^{2D}}$, taken by itself plots as an ideal 2D circle with centre on the horizontal Z'_{xy} axis. The intersections of the circle with the axis give the values of the TE and TM impedances for this (now artificially) ideal tensor.

Thus the common practice with MT data, when seeking TE and TM values, of finding the maximum and minimum values of Z'_{xy} as the observing axes are rotated, can be seen to be tantamount to an assumption that the $\mathbf{Z^{s2}}$ part of the matrix be ignored, so that the circle for the $\mathbf{Z^{2D}}$ part indeed plots in ideal 2D form.

5.3 Eigenvalue analysis

Eigenvalues ζ_1 and ζ_2 of a matrix $\mathbf{Z}$ are found by solving the characteristic equation

$$\zeta^2 - (Z_{xx} + Z_{yy})\zeta + Z_{xx}Z_{yy} - Z_{xy}Z_{yx} = 0 \quad (21)$$

to obtain

$$\zeta_1, \zeta_2 = (Z_{xx} + Z_{yy})/2 \pm [(Z_{xx} + Z_{yy})^2 + 4(Z_{xy}Z_{yx} - Z_{xx}Z_{yy})]^{\frac{1}{2}}/2 \quad (22)$$

Three cases are possible and of interest. Each case will be discussed separately.

5.3.1 Eigenvalues are conjugate pairs

The first case occurs when

$$(Z_{xx} + Z_{yy})^2 + 4(Z_{xy}Z_{yx} - Z_{xx}Z_{yy}) < 0 \tag{23}$$

and the two roots of the conjugate equation form a conjugate pair. The product of the two roots, $\zeta_1\zeta_2$, will always be positive. An equivalent way of expressing Inequality 23 is as

$$(Z_{xx} - Z_{yy})^2 + 4Z_{xy}Z_{yx} < 0 \tag{24}$$

5.3.2 Eigenvalues are real and equal

The second case occurs when

$$(Z_{xx} + Z_{yy})^2 + 4(Z_{xy}Z_{yx} - Z_{xx}Z_{yy}) = 0 \tag{25}$$

The two roots of the conjugate equation are now both real (positive or negative), and equal. In fact

$$\zeta_1 = \zeta_2 = (Z_{xx} + Z_{yy})/2 \tag{26}$$

Again, the product of the two roots, $\zeta_1\zeta_2$, will be positive.

5.3.3 Eigenvalues are real and different

The third case occurs when

$$(Z_{xx} + Z_{yy})^2 + 4(Z_{xy}Z_{yx} - Z_{xx}Z_{yy}) > 0 \tag{27}$$

The two roots of the conjugate equation are now both real, different, and positive or negative depending on the signs of $(Z_{xx} + Z_{yy})$ and $(Z_{xx}Z_{yy} - Z_{xy}Z_{yx})$, the trace and determinant respectively of $\mathbf{Z}$.

The product of the two eigenvalues is given by

$$\zeta_1\zeta_2 = \det \mathbf{Z} \tag{28}$$

and is positive if det$\mathbf{Z}$ is positive, and negative if det$\mathbf{Z}$ is negative.

5.4 Eigenvalues on Mohr diagrams

The three eigenvalue cases discussed in the preceding three subsections are clearly defined when the data are plotted on Mohr diagrams. Eigenvalues which are real are shown graphically. The directions of their eigenvectors may be read from the diagrams remembering, in Fig. 2a, the $2\theta'$ anticlockwise rotation of the radial arm for, in Fig. 1, the θ' clockwise rotation of the axes.

Thus for the case of Section 5.3.1, circles which (as in Fig. 5a) do not touch the vertical axes obey Inequality 23. Their eigenvalues are complex conjugate pairs, and real eigenvectors for them do not exist.

Secondly, for the case discussed in Section 5.3.2, Fig. 5b shows a circle which is just touching both vertical axes, $Z'_{xy} = 0$ and $Z'_{yx} = 0$. The eigenvalues may be read off the Z'_{xx} axis, as

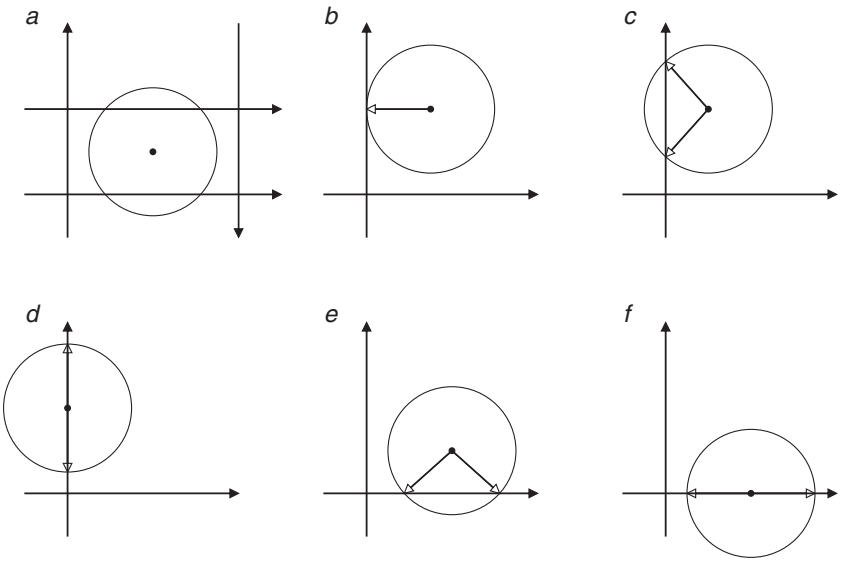

Fig. 5. Eigenvector directions (according to the radial arrows) and eigenvalues (where the arrowheads touch an axis) displayed on Mohr diagrams for a 2 x 2 matrix. a: Eigenvalues are complex conjugates, and are not evident on the diagram. b: Eigenvalues are real and equal; both eigenvectors are the same. c: Eigenvalues are real and different; eigenvectors are not orthogonal. d: Eigenvalues are real and different; eigenvectors are orthogonal. e: Associated MT eigenvalues are real and different; eigenvectors are not orthogonal. f: Associated MT eigenvalues are real and different; eigenvectors are orthogonal (the 2D case). In Fig. 5a axes are also drawn for Z'_{yx} and Z'_{yy}. Between the Z'_{xx} and Z'_{yy} axes, the product $Z'_{xy}.Z'_{yx} < 0$. On the Z'_{xx} and Z'_{yy} axes, $Z'_{xy}.Z'_{yx} = 0$. Outside the Z'_{xx} and Z'_{yy} axes, $Z'_{xy}.Z'_{yx} > 0$.

$(Z_{xx} + Z_{yy})/2$. The direction of the repeated eigenvector corresponds to the direction of a radial arm which is horizontal in the diagram, as shown.

Thirdly, for the case discussed in Section 5.3.3, in Fig. 5c a circle is shown which, like examples to be discussed below, now crosses the vertical axes. The two eigenvalues may again be read off the Z'_{xx} axis where the circle cuts this axis, and the two eigenvector directions are given by the θ' values for the radial arms to these points.

The example in Fig. 5c demonstrates that real eigenvalues correspond to the MT case of "phase going out of quadrant". Also it can be seen, by an extension of the discussion in Section 5.3.3 above, that for a Mohr circle to not capture the origin the product of the two eigenvalues must be positive; i.e. det$\mathbf{Z}$ must be positive.

Of equal interest in MT are the eigenvectors of the associated problem, which correspond to intersections of a circle with the horizontal Z'_{xy} axis. As shown in Fig. 5e, these might be regarded as an approximation to 2D TE and TM values, and for the true 2D case (Fig. 5f) they will indeed be so. These eigenvalues may be found by similar formalism, or by elementary trigonometry based on Fig. 2a. They may be evident from inspection, as in Lilley (1993).

6. Singular value decomposition

It is instructive also to apply SVD to an MT tensor, taking the in-phase and quadrature parts of the tensor separately.

As described for example by Strang (2005), decomposition by SVD factors a matrix $\mathbf{A}$ into

$$\mathbf{A} = \mathbf{U}\boldsymbol{\Sigma}\mathbf{V}^{\mathbf{T}} \tag{29}$$

where the columns of $\mathbf{V}$ are eigenvectors of $\mathbf{A}^{\mathbf{T}}\mathbf{A}$, and $\mathbf{A}^{\mathbf{T}}$ denotes the transpose of $\mathbf{A}$. The columns of $\mathbf{U}$ (which are eigenvectors of $\mathbf{A}\mathbf{A}^{\mathbf{T}}$) may be found by multiplying $\mathbf{A}$ by the columns of $\mathbf{V}$. The singular values on the diagonal of $\boldsymbol{\Sigma}$ are the square roots (taken positive by convention, a most important point in the present context) of the non-zero eigenvalues of $\mathbf{A}\mathbf{A}^{\mathbf{T}}$. As $\boldsymbol{\Sigma}$ is diagonal, it is straightforward to convert it to the antidiagonal form of an ideal 2D tensor, for example by expressing Equation 29 as

$$\mathbf{A} = \mathbf{U}\boldsymbol{\Sigma}\mathbf{W}\mathbf{W}^{-\mathbf{1}}\mathbf{V}^{\mathbf{T}} \tag{30}$$

where $\mathbf{W} = [0, 1; -1, 0]$ and $\mathbf{V}^{\mathbf{T}}$ is pre-multiplied by $\mathbf{W}^{-\mathbf{1}}$, with $\mathbf{W}^{-\mathbf{1}}$ denoting the inverse of $\mathbf{W}$.

Equations for this form of the SVD of an MT tensor were derived in an earlier paper (Lilley, 1998). Taking phase relative to the $\mathbf{H}$ signal, so that $\mathbf{H}_q$ is zero, Equation 1 is written in its in-phase and quadrature parts as

$$\mathbf{E}_{p,q} = \mathbf{R}(-\theta e_{p,q}) \begin{bmatrix} 0 & \Upsilon_{p,q} \\ -\Psi_{p,q} & 0 \end{bmatrix} \mathbf{R}(\theta h_{p,q})\mathbf{H} \tag{31}$$

where the electric and magnetic observation axes are rotated clockwise independently, the electric axes by $\theta e_{p,q}$ and the magnetic axes by $\theta h_{p,q}$. Thus the in-phase part of the tensor, $\mathbf{Z}_p$, is factored into

$$\begin{bmatrix} Z_{xx_p} & Z_{xy_p} \\ Z_{yx_p} & Z_{yy_p} \end{bmatrix} = \mathbf{R}(-\theta e_p) \begin{bmatrix} 0 & \Upsilon_p \\ -\Psi_p & 0 \end{bmatrix} \mathbf{R}(\theta h_p) \tag{32}$$

where

$$\theta e_p = \frac{1}{2}\left[\arctan\frac{Z_{yy_p} - Z_{xx_p}}{Z_{xy_p} + Z_{yx_p}} + \arctan\frac{Z_{yy_p} + Z_{xx_p}}{Z_{xy_p} - Z_{yx_p}}\right] \tag{33}$$

$$\theta h_p = \frac{1}{2}\left[\arctan\frac{Z_{yy_p} - Z_{xx_p}}{Z_{xy_p} + Z_{yx_p}} - \arctan\frac{Z_{yy_p} + Z_{xx_p}}{Z_{xy_p} - Z_{yx_p}}\right] \tag{34}$$

$$\Upsilon_p - \Psi_p = \cos(\theta e_p + \theta h_p)[(Z_{xy_p} + Z_{yx_p}) - \tan(\theta e_p + \theta h_p)(Z_{xx_p} - Z_{yy_p})] \tag{35}$$

and

$$\Upsilon_p + \Psi_p = \cos(\theta e_p - \theta h_p)[(Z_{xy_p} - Z_{yx_p}) + \tan(\theta e_p - \theta h_p)(Z_{xx_p} + Z_{yy_p})] \tag{36}$$

(Equation 36 corrects equation 22 of Lilley (1998), where a negative sign is missing.) A similar set to Equations 32, 33, 34, 35 and 36 applies for the quadrature part of a tensor, with subscript q replacing p.

The quantities $\Upsilon_{p,q}$ and $\Psi_{p,q}$ are termed principal values. An examination of the possibility that one or both of $\Psi_{p,q}$ may be zero or negative is addressed in Section 13.3.

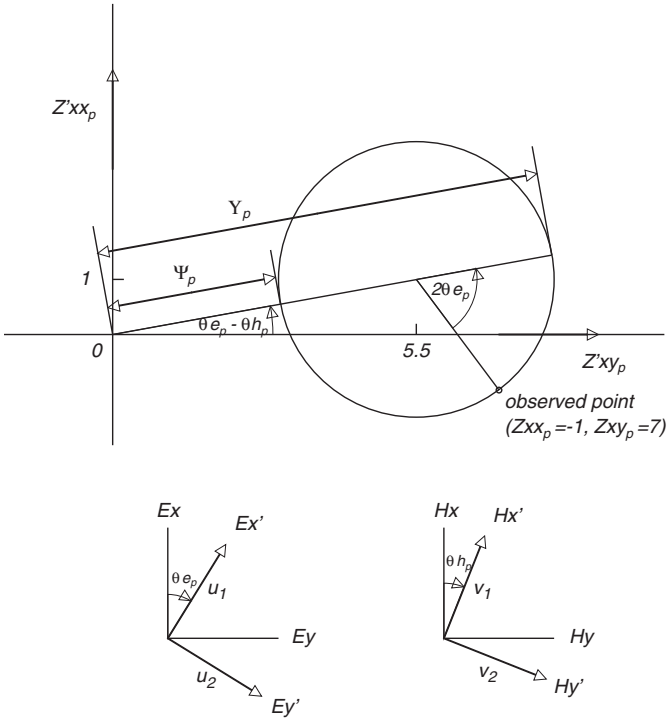

Fig. 6. Diagram showing the Mohr representation and the SVD of the matrix in Equation 37. The values of θe_p, θh_p, Υ_p and Ψ_p are evident as $32^\circ, 21^\circ$, 8.1 and 3.1. The axes for E'_x, E'_y and H'_x, H'_y show the rotations, from E_x, E_y and H_x, H_y by θe_p and θh_p respectively, to give an ideal 2D antidiagonal response.

The quantities arising from the SVD may be displayed on a Mohr diagram as in Fig. 6, which has been drawn for a tensor

$$\mathbf{Z}_p = [-1,7; -4,3] \tag{37}$$

The values of θe_p, θh_p, Υ_p and Ψ_p may be evaluated by the equations above as $31.7^\circ, 21.4^\circ$, 8.09 and 3.09 respectively. These values may also be read off the figure.

When the matrix of Equation 37 is put into a standard computing routine, the SVD returned is commonly in the form of Equation 29:

$$\mathbf{Z}_p = \begin{bmatrix} -.8507 & -.5257 \\ -.5257 & .8507 \end{bmatrix} \begin{bmatrix} 8.0902 & 0 \\ 0 & 3.0902 \end{bmatrix} \begin{bmatrix} .3651 & -.9310 \\ -.9310 & -.3651 \end{bmatrix} \tag{38}$$

which may be given the form of Equation 32 by expressing it first as

$$\mathbf{Z}_p = \begin{bmatrix} .8507 & -.5257 \\ .5257 & .8507 \end{bmatrix} \begin{bmatrix} 0 & 8.0902 \\ -3.0902 & 0 \end{bmatrix} \begin{bmatrix} .9310 & .3651 \\ -.3651 & .9310 \end{bmatrix} \tag{39}$$

and then as

$$\mathbf{Z}_p = \begin{bmatrix} \cos 31.71^\circ & -\sin 31.71^\circ \\ \sin 31.71^\circ & \cos 31.71^\circ \end{bmatrix} \begin{bmatrix} 0 & 8.0902 \\ -3.0902 & 0 \end{bmatrix} \begin{bmatrix} \cos 21.41^\circ & \sin 21.41^\circ \\ -\sin 21.41^\circ & \cos 21.41^\circ \end{bmatrix} \quad (40)$$

The columns of the first matrix $[\cos 31.71^\circ, -\sin 31.71^\circ; \sin 31.71^\circ, \cos 31.71^\circ]$, which have been derived from $\mathbf{U}$ in Equation 29, can be seen to define unit vectors u_1 and u_2 which are as given for E'_x and E'_y in Fig. 6. The rows of the third matrix $[\cos 21.41^\circ, \sin 21.41^\circ; -\sin 21.41^\circ, \cos 21.41^\circ]$, which have been derived from $\mathbf{V^T}$ in Equation 29, can be seen to define unit vectors v_1 and v_2 as given for H'_x and H'_y in Fig. 6. Also, as is evident, the singular values in the diagonal of matrix $\mathbf{\Sigma}$ (the second matrix) give the values of Υ_p and Ψ_p.

Note that by rotation of the electric and magnetic axes separately, the MT tensor has been reduced to an ideal 2D form. In a search for the nearest 2D model in a 3D situation the results of SVD may be valuable to bear in mind; the magnetic axes may be an indication of regional strike, with the electric axes showing the brunt of the distortion. A disadvantage of such an analysis however is that a rather artificial conductivity structure is required to simply twist the electric field at an observing site to explain the different rotations required of the E and H axes. A more specific (if simple) model for local distortion is widely accepted, and will be discussed in Section 11. With this model, in the case of near-singular MT data, it will be shown that a surficial strike direction is determined. However regional strike determination remains possible if regional anisotropy is high.

7. A condition number to measure singularity in an MT tensor

It is common experience to find very strong anisotropy in an observed tensor, both for distorted 2D cases, and indeed generally. As a consequence, the tensor approaches a condition of singularity, in both its in-phase and quadrature parts. In a Mohr diagram the condition of singularity is shown by a circle touching the origin. If for example $\mathbf{Z}_p$ is a singular tensor, then there is some rotation of axes for which both Z'_{xx_p} and Z'_{xy_p} are zero (or indistinguishable from zero, when error is taken into account). For the student of linear algebra, an example of a null space occurs: it is the line of the direction of nil electric field change, holding for all magnetic field changes.

A condition number may be used to warn that singularity is being approached (Strang, 2005). When the condition number becomes high in some sense, the matrix is said to be ill-conditioned (Press et al., 1989). The condition number suggested by Strang (2005) is the norm of the matrix (sometimes called the spectral norm) multiplied by the norm of the inverse of the matrix; or equivalently, the greater principal value of the matrix divided by the lesser principal value. For the 2 x 2 matrix $\mathbf{Z}$ in Equation 1 the condition numbers $\kappa_{p,q}$ are

$$\kappa_{p,q} = \Upsilon_{p,q} / |\Psi_{p,q}| \quad (41)$$

The greater and lesser principal values $\Upsilon_{p,q}$ and $\Psi_{p,q}$ are given by Equations 35 and 36 and, as discussed above, are the singular values of the matrix. Following the convention that singular values are never negative, a modulus sign is put into the denominator of Equation 41 to cover cases where computation of the lesser principal value produces a negative number. In terms

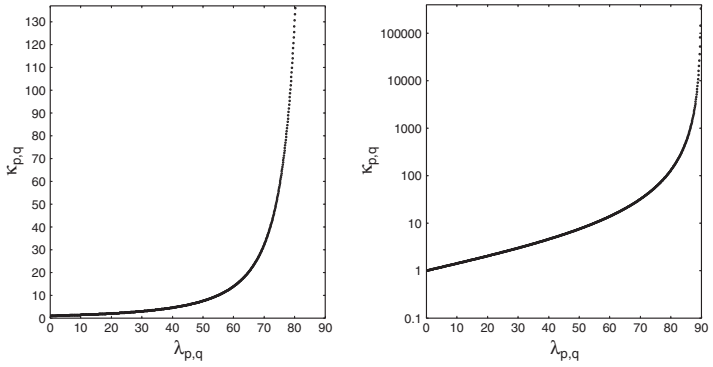

Fig. 7. The condition number $\kappa_{p,q}$ displayed as a function of the anisotropy angle $\lambda_{p,q}$ in degrees, using linear (left) and logarithmic (right) scales for $\kappa_{p,q}$.

of the Mohr representations in Figs 2, 3 and 6, from Equation 41 the condition numbers are given by

$$\kappa_{p,q} = (Z^L_{p,q} + C_{p,q})/|(Z^L_{p,q} - C_{p,q})| \tag{42}$$

that is

$$\kappa_{p,q} = 2/(\csc\lambda_{p,q} - 1) + 1 \tag{43}$$

remembering Equation 16. Fig. 7 shows $\kappa_{p,q}$ as a function of $\lambda_{p,q}$. While $\lambda_{p,q}$ itself is a measure of condition, Fig. 7 demonstrates that $\kappa_{p,q}$ is more sensitive than $\lambda_{p,q}$ as ill-condition is approached. Note that $\kappa_{p,q} \geq 1$.

An example is given in Fig. 8 of condition numbers determined for a set of data from a recent MT site, NQ142, in north Queensland, Australia. An increase in condition number above 10 monitors the decrease of the lesser principle value $\Psi_{p,q}$, which becomes negligible. The variation of angle $\theta e_{p,q}$ with period (T) stabilizes as condition numbers rise, an effect discussed below in Section 11.

8. The phase tensor

Caldwell et al. (2004) introduced a "phase tensor" based on the magnetotelluric tensor, and the concept was further developed by Bibby et al. (2005). The phase tensor is a real matrix $\mathbf{\Phi}$, defined by

$$\mathbf{\Phi} = \mathbf{Z_p^{-1}Z_q} \tag{44}$$

and it has the property that it is unaffected by the in-phase distortion (described in Section 11.1 below) which is recognised as common in MT data. Note, however, that the computation of phase tensor values may encounter difficulties for high condition numbers and singularities in $\mathbf{Z_p}$ and $\mathbf{Z_q}$, which can be caused by strong distortion.

8.1 Mohr diagram for the phase tensor

The phase tensor, a 2 x 2 matrix, can also be represented by a Mohr diagram, as described by Weaver et al. (2003; 2006). The general form is shown in Fig. 9, following the convention for axes of Fig. 2a. Equations 6 to 15 can be adapted to apply to the quantities shown in Fig. 9.

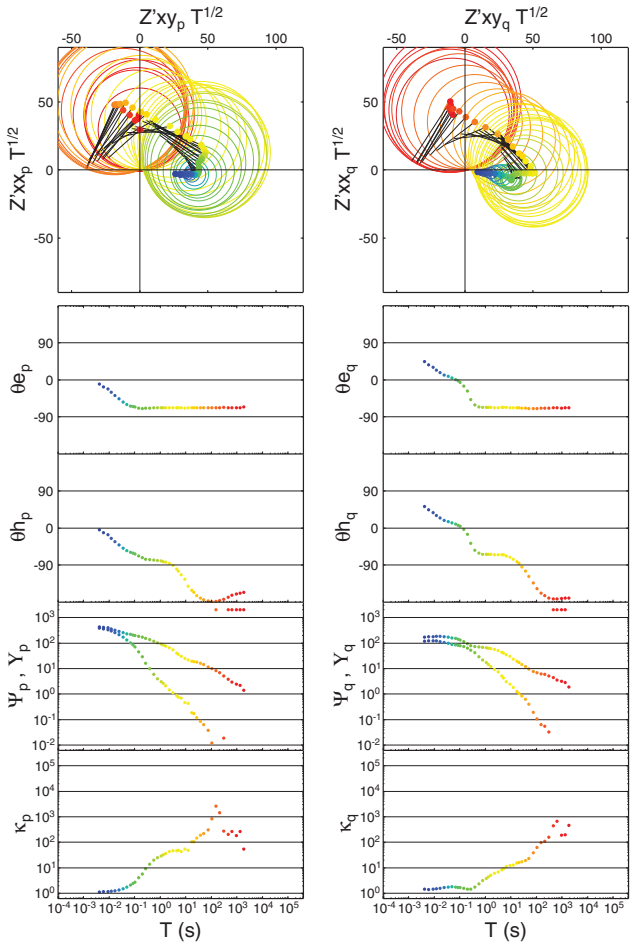

Fig. 8. The NQ142 data plotted as Mohr diagrams and analysed by SVD to give: angles θe_p, θe_q, θh_p and θh_q; the principal values Υ_p, Ψ_p, Υ_q and Ψ_q; and the condition numbers κ_p and κ_q. The variation of period with colour in the circles is the same as for the other plots. The Mohr diagrams follow the form of Fig. 2a, and have their impedance values multiplied by the square root of period (T) to make the plots more compact. Where circles enclose the origin, their lesser principal value (Ψ) is given an artificially high value to flag this circumstance; however condition numbers are computed nevertheless.

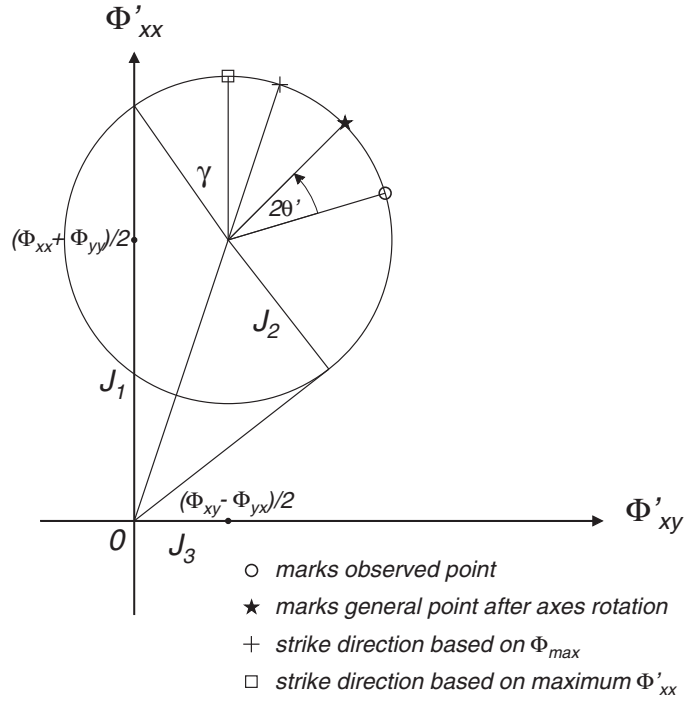

Fig. 9. Diagram showing the Mohr representation of the general phase tensor. Axes for Φ'_{yy} and Φ'_{yx} could be added (following Fig. 2a). The principal values (equivalent to Υ_p and Ψ_p in Fig. 6) are given by $({J_1}^2 + {J_3}^2)^{1/2} \pm J_2$, and are denoted Φ_{max} and Φ_{min} by Caldwell et al. (2004).

The angle γ, which is a measure of 3D effects, is the seventh invariant of Weaver et al. (2000), described in Section 4.

The regional 2D strike direction chosen on phase considerations, as advocated by Bahr (1988) for example, is given by the point of maximum Φ'_{xx}, which is the highest point of the circle as drawn. However when the regional structure is recognised as being 3D, the best estimate of geologic strike is recommended by Caldwell et al. (2004) as the orientation of the principal axes of the phase tensor, shown in Fig. 9 as "strike direction based on Φ_{max}".

Note that a Mohr diagram for the phase tensor shows the variation of phase-tensor values as the observing axes are rotated, but that these values are generally not those of the usual MT Z_{xy} phase.

Also note that a Z_{xy} phase going "out of quadrant" does not imply that a principal value of $\mathbf{\Phi}$ is negative. In fact det$\mathbf{\Phi}$ is expected to be never negative, consistent with the principal values of $\mathbf{\Phi}$ (Φ_{max} and Φ_{min}) being never negative.

Examples of Mohr diagrams for phase tensors, which illustrate some of these points, are given in Lilley & Weaver (2010).

8.2 Mohr diagram for the 2D phase tensor

For the 2D case, the Mohr diagram reduces to a circle with centre on the Φ'_{xx} axis. The TE and TM phase values are then the arctangents of the intercepts which, from the analysis already given, are eigenvalues of the phase tensor. The two eigenvectors are orthogonal.

8.3 Mohr diagram for the 1D phase tensor

For the 1D case, the Mohr diagram reduces to a point on the Φ'_{xx} axis, marking the tangent of the phase value of the 1D MT response.

9. Invariants for the general phase tensor

To characterize the phase tensor just three invariants of rotation are needed, as pointed out by Caldwell et al. (2004), together with an angle defining the direction of the original observing axes. Options for invariants are evident from an inspection of Fig. 9, and include those adopted in Section 4 for Fig. 3. Weaver et al. (2003) chose J_1, J_2 and J_3 as shown in Fig. 9, which neatly summarize 1D, 2D and 3D characteristics, respectively.

10. Some complications illustrated by Mohr diagrams

10.1 Conditions for Z_{xy} and Z_{yx} phases out of quadrant

For simple cases of induction in 1D layered media, Z_{xy} phases will be in the first quadrant, and Z_{yx} phases in the third quadrant. However, it is not uncommon with complicated geologic structure to find phases which are out of these expected quadrants, for some orientation of the measuring axes. Experimental or computational error may be invoked in explanation, when in fact a common cause is simply distortion. Such distortion may be understood by reference to Fig. 3. Clearly once, due say to distortion, angle μ_p (or μ_q) increases to the point where the in-phase (or quadrature) circle first touches and then crosses the vertical Z'_{xx} axis, for an appropriate direction of the observing axes the phase observed of Z_{xy} will be "out of quadrant".

Adopting, in the rotated frame, the common definition for phase ϕ'_{xy} of

$$\phi'_{xy} = \arctan(Z'_{xy_q}/Z'_{xy_p}) \tag{45}$$

where the signs of numerator and denominator are taken into account, then ϕ'_{xy} is in the first quadrant when both Z'_{xy_p} and Z'_{xy_q} are positive.

The condition for the phase of Z'_{xy} to go out of quadrant is that one or both of its in-phase and quadrature parts should be negative. On the Mohr circle diagram, this condition is equivalent to either or both of the in-phase and quadrature circles for the data crossing the vertical axis. Phases greater than 90° are then possible for Z'_{xy}. If the circles however remain to the right of their vertical axes, the Z'_{xy} phase will be in quadrant for any orientation of the measuring axes.

With reference to Fig. 3, for the crossing of the vertical axis to occur, it can be seen that $\lambda_{p,q}$ and $\mu_{p,q}$ must together be greater than 90°, i.e.

$$\lambda_{p,q} + |\mu_{p,q}| > 90^\circ \tag{46}$$

With reference to the Z'_{yy_p} and Z'_{yx_p} axes also included in Fig. 2a, consequences for the phases of other elements are also clear. The symmetry of the figure is such that if the circle crosses the Z'_{xx_p} axis to the left, it will also cross the Z'_{yy_p} axis to the right. Thus if phases out of quadrant are possible for Z'_{xy}, so are they also possible for Z'_{yx}. However, the latter will occur for rotations 90° different from the former.

Similar considerations will give rules regarding the quadrants to be expected for Z'_{xx} and Z'_{yy} phases. An analysis of Fig. 2a shows that these phases will generally change quadrant with a rotation of the observing axes. An exception, when they would not do so, would be if the circle in Fig. 2a did not cross the horizontal Z'_{xy_p} axis, but stayed completely above (or below) this axis (and the circle for the quadrature part of the tensor behaved similarly).

10.2 Strike coordinates from phase considerations

The situation of Z_{xy} phase out of quadrant (for example for the part of the circle to the left of the vertical axis in Fig. 5c) causes difficulty in the symmetric-antisymmetric and the symmetric-2D partitions of Sections 5.1 and 5.2. First, if the circle in Fig. 5c is simply moved down so that its centre lies on the horizontal axis, the left-hand intercept with the horizontal axis is less than zero. The circle has enclosed the origin, and a negative value is obtained for the lesser of TE and TM, contrary to expectation (see Section 13.1).

Similarly there are methods which seek, as geologic strike coordinates, those given by maximum and minimum Z'_{xy} phase values when the axes are rotated. These methods will find erratic phase behaviour when either or both of the in-phase and quadrature circles cross the vertical axis as in Fig. 5c.

However Z'_{xy} phase will usually be at or near a maximum (or minimum) at the right-hand side of a circle which on its left-hand side crosses the vertical axis. Thus sensible results for maximum or minimum phase can be expected, if based only on a determination from the right-hand side.

11. Geologic interpretation of angles found by SVD, when condition numbers are high

Singular value decomposition of observed magnetotelluric tensors, taking the in-phase and quadrature parts separately, often produces directions which are frequency independent below a certain frequency which is found to be common to both in-phase and quadrature parts. This section examines how such directions may be related to the angles which arise in basic distortion models of MT data. It is found that while MT data are expected in general to be frequency dependent, there are particular limiting cases which are constant with frequency. Understanding such observed data may be useful in interpretation.

11.1 The Smith (1995) model for local distortion

This section applies the Smith (1995) description of local "static" distortion, which follows Bahr (1988) and Groom & Bailey (1989). In the absence of local distortion the measured magnetic field $\mathbf{H}$ is related to the regional electric field $\mathbf{E^r}$ by the tensor $\mathbf{Z^r}$:

$$\mathbf{E^r} = \mathbf{Z^r H} \tag{47}$$

and with distortion $\mathbf{d}$ present, affecting the measured electric field $\mathbf{E^m}$ only,

$$\mathbf{E^m} = \mathbf{d}\mathbf{E^r} \tag{48}$$

and

$$\mathbf{E^m} = \mathbf{Z^m}\mathbf{H} = \mathbf{d}\mathbf{Z^r}\mathbf{H} \tag{49}$$

For the case of 2D regional structure, with measuring axes aligned with regional strike,

$$\tilde{\mathbf{Z}}^{\mathbf{r}} = [0, Z^r_{12}; Z^r_{21}, 0] \tag{50}$$

and so

$$\tilde{\mathbf{E}}^{\mathbf{m}} = \mathbf{d}[0, Z^r_{12}; Z^r_{21}, 0]\mathbf{H} \tag{51}$$

where the overscore˜indicates observing axes aligned with regional strike.

If the observation axes are north-south and east-west, say, and need to be rotated angle θ for alignment with regional strike, then Equation 51 (without distortion) gives

$$\mathbf{R}(\theta)\begin{bmatrix} E^m_x \\ E^m_y \end{bmatrix} = \begin{bmatrix} 0 & Z^r_{12} \\ Z^r_{21} & 0 \end{bmatrix}\mathbf{R}(\theta)\begin{bmatrix} H_x \\ H_y \end{bmatrix} \tag{52}$$

and with distortion

$$\mathbf{R}(\theta)\begin{bmatrix} E^m_x \\ E^m_y \end{bmatrix} = \mathbf{d}\begin{bmatrix} 0 & Z^r_{12} \\ Z^r_{21} & 0 \end{bmatrix}\mathbf{R}(\theta)\begin{bmatrix} H_x \\ H_y \end{bmatrix} \tag{53}$$

In co-ordinates aligned with the surficial geology the distortion amounts to scaling the electric fields by different amounts, g_1 and g_2, in directions parallel and perpendicular to the surficial strike (Zhang et al., 1987). Distortion matrix $\mathbf{d}$ then has the form

$$\begin{bmatrix} d_{11} & d_{12} \\ d_{12} & d_{22} \end{bmatrix} = \mathbf{R}(-\alpha_s)\begin{bmatrix} g_1 & 0 \\ 0 & g_2 \end{bmatrix}\mathbf{R}(\alpha_s) \tag{54}$$

where due to the restricted distortion model the d_{21} element has the value d_{12}, g_1 and g_2 are real constants (frequency independent), and α_s is the angle from the regional strike coordinates to the strike coordinates of the surficial structure causing the distortion. The decomposition of $\mathbf{d}$ in Equation 54 is displayed in Fig. 10.

Substituting the expression for $\mathbf{d}$ from Equation 54 into Equation 53 gives

$$\mathbf{E^m} = \mathbf{R}(-\theta - \alpha_s)\begin{bmatrix} g_1 Z^r_{21}\sin\alpha_s & g_1 Z^r_{12}\cos\alpha_s \\ g_2 Z^r_{21}\cos\alpha_s & -g_2 Z^r_{12}\sin\alpha_s \end{bmatrix}\mathbf{R}(\theta)\mathbf{H} \tag{55}$$

At this stage the in-phase and quadrature parts can be considered separately. Avoiding the encumbrance of additional notation, now assume that just the in-phase part of the measured E field is being considered, giving information on just the in-phase parts of the regional impedance tensor $\mathbf{Z^r}$.

Then following the form of Equation 32, SVD can be carried out on the central tensor in Equation 55, expanding it as

$$\begin{bmatrix} g_1 Z^r_{21}\sin\alpha_s & g_1 Z^r_{12}\cos\alpha_s \\ g_2 Z^r_{21}\cos\alpha_s & -g_2 Z^r_{12}\sin\alpha_s \end{bmatrix} = \mathbf{R}(-\eta_e)\begin{bmatrix} 0 & \Upsilon \\ -\Psi & 0 \end{bmatrix}\mathbf{R}(\eta_h) \tag{56}$$

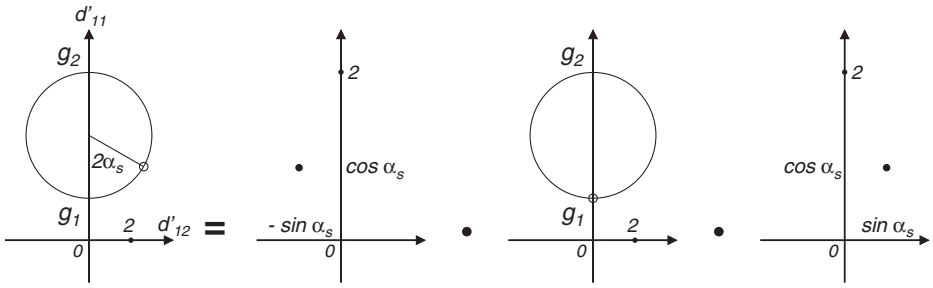

Fig. 10. Mohr diagrams for the decomposition in Equation 54. On the left the diagram shows the distortion matrix **d**. It is positive definite, due to the assumption of strictly 2D surficial anisotropy, and so has orthogonal eigenvectors. The radius of the circle is $(g_2 - g_1)/2$. The numerical matrix taken for the example is [3.5, 2.6; 2.6, 6.5], and the directions and magnitudes of its eigenvectors are shown by rotating the radial arm until it is parallel to the vertical axis. The eigenvalues then are $g_1 = 2$ and $g_2 = 8$. The angle $2\alpha_s$ on the figure is 60°, indicating that a rotation of axes anticlockwise through 30° is necessary to change the matrix to [2, 0: 0, 8]. On the right is shown the matrix decomposition as in Equation 54. The three diagrams represent the three matrices on the right-hand side of that equation, in turn. The first Mohr diagram represents a rotation by angle $(-\alpha_s)$. The second Mohr diagram is symmetric, representing a positive definite matrix according to the scaling factors g_1 and g_2. The third matrix is like the first, representing a rotation by angle $(+\alpha_s)$. Note the changes of scale between the diagrams.

where the angles η_e and η_h, and the principal values Y and Ψ are given by

$$\eta_e + \eta_h = \arctan\left[\frac{-g_2 Z_{12}^r \sin\alpha_s - g_1 Z_{21}^r \sin\alpha_s}{g_1 Z_{12}^r \cos\alpha_s + g_2 Z_{21}^r \cos\alpha_s}\right] \tag{57}$$

$$\eta_e - \eta_h = \arctan\left[\frac{-g_2 Z_{12}^r \sin\alpha_s + g_1 Z_{21}^r \sin\alpha_s}{g_1 Z_{12}^r \cos\alpha_s - g_2 Z_{21}^r \cos\alpha_s}\right] \tag{58}$$

$$\mathrm{Y} + \Psi = [(g_1 Z_{21}^r \sin\alpha_s - g_2 Z_{12}^r \sin\alpha_s)^2 + (g_2 Z_{21}^r \cos\alpha_s - g_1 Z_{12}^r \cos\alpha_s)^2]^{1/2} \tag{59}$$

and

$$\mathrm{Y} - \Psi = [(g_1 Z_{21}^r \sin\alpha_s + g_2 Z_{12}^r \sin\alpha_s)^2 + (g_1 Z_{12}^r \cos\alpha_s + g_2 Z_{21}^r \cos\alpha_s)^2]^{1/2} \tag{60}$$

Replacing into Equation 55 the matrix in its expanded form as in Equation 56, and combining adjoining rotation matrices, gives

$$\mathbf{E^m} = \mathbf{R}(-\theta - \alpha_s - \eta_e)\begin{bmatrix} 0 & \mathrm{Y} \\ -\Psi & 0 \end{bmatrix}\mathbf{R}(\theta + \eta_h)\mathbf{H} \tag{61}$$

Thus in the SVD of an MT tensor resulting from 2D surficial distortion of a regional 2D structure, the regional strike θ and the various distortion quantities g_1, g_2 and α_s occur in a way which does not allow their straightforward individual solution, because the SVD produces values for $(\theta + \alpha_s + \eta_e)$ and $(\theta + \eta_h)$. It is of interest however to examine two limiting cases, as in the following sections.

11.2 First limiting case

Now consider, in Equations 57, 58, 59 and 60, that $g_2 \gg g_1$, so that terms in g_1 are ignored with respect to terms in g_2. The results are then obtained that

$$\Upsilon = g_2[(Z^r_{12}\sin\alpha_s)^2 + (Z^r_{21}\cos\alpha_s)^2]^{1/2} \tag{62}$$

and

$$\Psi = 0 \tag{63}$$

For the angles η_e and η_h the limiting case gives

$$\eta_e = 0 \tag{64}$$

and

$$\eta_h = -\arctan(Z^r_{12}\tan\alpha_s / Z^r_{21}) \tag{65}$$

While in Equation 65 for η_h the values Z^r_{12}, Z^r_{21} and α_s still occur together, for η_e there is the simple result of zero. Fed back into Equation 61 it is seen that SVD of an MT tensor now gives, in the equivalent of θe in Equation 31, a result for $(\theta + \alpha_s)$: that is, the direction of surficial 2D strike.

Further, note that if $Z^r_{12}/Z^r_{21} = -1$, then $\eta_h = \alpha_s$, and the magnetic axes are also aligned with (or normal to) the surficial strike. This case can be seen to be that where the regional 2D anisotropy is out-weighed by the surficial anisotropy, so that the former approximates a 1D case.

11.3 Second limiting case

A second limiting case might be gross inequality in the TE and TM components of the regional 2D impedance. Consider the case where $|Z^r_{12}| \gg |Z^r_{21}|$, so that terms involving the latter may be ignored with respect to terms involving the former. Then Equations 57, 58, 59 and 60 give

$$\Upsilon = Z^r_{12}[(g_2\sin\alpha_s)^2 + (g_1\cos\alpha_s)^2]^{1/2} \tag{66}$$

and

$$\Psi = 0 \tag{67}$$

For the angles η_e and η_h this limiting case gives

$$\eta_e = -\arctan(g_2\tan\alpha_s / g_1) \tag{68}$$

and

$$\eta_h = 0 \tag{69}$$

Fed back into Equation 61, it is seen that SVD of an MT tensor for the case where $\eta_h = 0$ now gives, in the equivalent of θh in Equation 31, a result for θ: that is, the direction of regional 2D strike.

12. Discussion and example

The two limiting cases, where realised, give angles of interest. Also, it should be noted that both cases correspond to the MT tensor being singular, or nearly so.

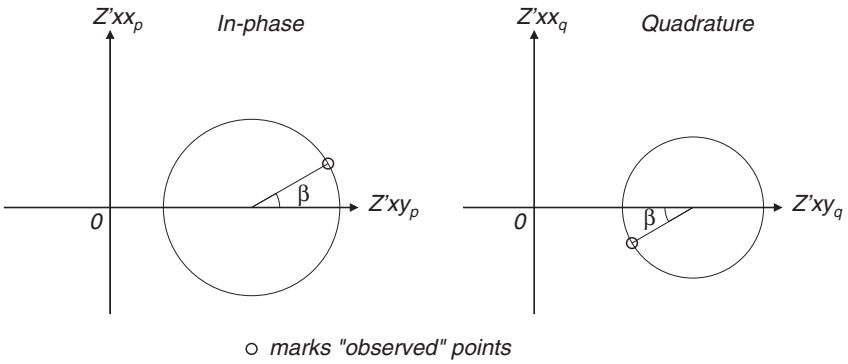

Fig. 11. Hypothetical example of a 2D case with the in-phase and quadrature radial arms anti-parallel. Such cases appear to be prohibited in nature, but inadvertently can be posed as numerical examples.

The example in Fig. 8, for frequencies less that 10 Hz, gives $\theta e_{p,q}$ values which are fixed at -67°, while $\theta h_{p,q}$ values continue to vary with period. The model of Section 11.1 is therefore a good candidate for the interpretation of the data. Applying the results of Section 11.2, surficial strike is determined at -67° ($\pm 90^\circ$ allowing for the usual ambiguity).

However the observation that there is a critical frequency, say f_c, only below which $\theta e_{p,q}$ values are frequency independent (and in the case of Fig. 8 are stable at -67°), implies a contradiction to the initial distortion model in Section 11.1, which was frequency independent, generally. The existence of such a "critical frequency" suggests distortion which is "at a distance", rather than immediately local.

13. Some remaining problems

13.1 TE and TM modes both positive?

It is well known that for the 2D case the TM mode is always positive (Weidelt & Kaikkonen, 1994), but proof has not been achieved for the TE case. It can be seen from Fig. 2b that were the TE case to be negative in either in-phase or quadrature part (or both) then the appropriate circles would enclose their origin of axes. Thus a general proof that circles cannot enclose their origins (discussed in Section 13.3 below) would also prove that the TE mode can never be negative.

13.2 Radial arms anti-parallel

The 2D example given in Fig. 2b, where the in-phase and quadrature radial arms are parallel, represents the common case observed without exception in the experience of the present author. However, in principle the case shown in Fig. 11 where the in-phase and quadrature radial arms are anti-parallel would also be two dimensional. If there is a theoretical reason why cases with radial arms anti-parallel as in Fig. 11 do not occur in practice it would be an advance to have it clarified.

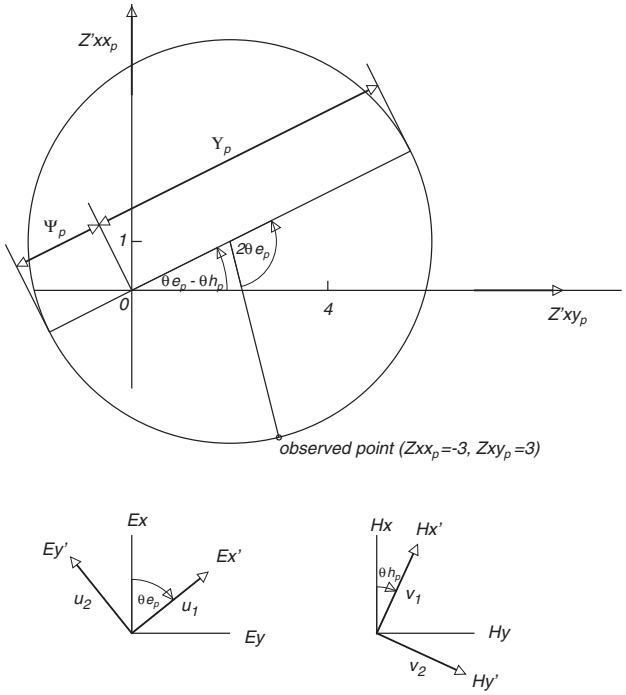

Fig. 12. The Mohr diagram for the matrix in Equation 70. The circle encloses the origin of axes because the matrix has a negative determinant. The values of θe_p, θh_p, Y_p and Ψ_p are evident as $51^\circ, 25^\circ, 6.3$ and -1.8 (Ψ_p being of negative sign when the direction of Y_p from the origin defines positive).

13.3 Circles capturing the origin: a note on negative determinants

It is also observed that circles do not capture or enclose their origins of axes, except for reasons of obvious error, or usual errors associated with singularity. The author suggests that this observed behaviour corresponds to the prohibition of components of negative resistivity in the electrical conductivity structure. Again a proof regarding this possibility would be welcome.

Negative determinants (no matter how they arise) need care in their analysis, as the following example illustrates. If, in contrast to the example in Section 6, the determinant (say of $\mathbf{Z}_p$) is negative, then the matrices $\mathbf{Z}_p\mathbf{Z}_p^{\mathbf{T}}$ and $\mathbf{Z}_p^{\mathbf{T}}\mathbf{Z}_p$ will each have a negative eigenvalue. However in a conventional SVD these negative eigenvalues are taken as positive singular values, and to allow for this action the sign is also changed of the eigenvector of $\mathbf{U}$ which they multiply.

To demonstrate this point, consider the hypothetical matrix

$$\mathbf{Z}_p = [-3, 3; -1, 5] \tag{70}$$

which has a negative determinant. The Mohr diagram representation of the matrix is shown in Fig. 12.

By Equations 33, 34, 35 and 36, the values of θe_p, θh_p, Υ_p and Ψ_p are evaluated as $51.26^\circ, 24.70^\circ, 6.36$ and -1.88 respectively. As before, by multiplying out the right-hand side, it can be checked that these values do indeed satisfy Equation 32. Also these values may be read off Fig. 12 as $51^\circ, 25^\circ, 6.3$ and -1.8, but now difficulties arising from the negative determinant are evident. Taking the direction of Υ_p from the origin to define positive, the value of Ψ_p is seen to be negative.

Put into a standard computing routine, the SVD returned for the matrix in Equation 70 is

$$\mathbf{Z}_p = \begin{bmatrix} .6257 & .7800 \\ .7800 & -.6257 \end{bmatrix} \begin{bmatrix} 6.3592 & 0 \\ 0 & 1.8870 \end{bmatrix} \begin{bmatrix} -.4179 & .9085 \\ -.9085 & -.4179 \end{bmatrix} \tag{71}$$

which may also be obtained formally by determining the eigenvalues and eigenvectors of $\mathbf{Z}_p^{\mathbf{T}}\mathbf{Z}_p$. To give it the form of Equation 32, Equation 71 may be expressed

$$\mathbf{Z}_p = \begin{bmatrix} .6257 & .7800 \\ .7800 & -.6257 \end{bmatrix} \begin{bmatrix} 0 & 6.3592 \\ -1.8870 & 0 \end{bmatrix} \begin{bmatrix} .9085 & .4179 \\ -.4179 & .9085 \end{bmatrix} \tag{72}$$

and then written

$$\mathbf{Z}_p = \begin{bmatrix} \cos 51.26^\circ & \sin 51.26^\circ \\ \sin 51.26^\circ & -\cos 51.26^\circ \end{bmatrix} \begin{bmatrix} 0 & 6.3592 \\ -1.8870 & 0 \end{bmatrix} \begin{bmatrix} \cos 24.70^\circ & \sin 24.70^\circ \\ -\sin 24.70^\circ & \cos 24.70^\circ \end{bmatrix} \tag{73}$$

The rows of the third matrix $[\cos 24.70^\circ, \sin 24.70^\circ; -\sin 24.70^\circ, \cos 24.70^\circ]$ define unit vectors v_1 and v_2 for H'_x, H'_y as shown in Fig. 12. As for Fig. 6, these indicate a rotation of the H_x, H_y observing axes.

However, the columns of the first matrix $[\cos 51.26^\circ, \sin 51.26^\circ; \sin 51.26^\circ, -\cos 51.26^\circ]$ define unit vectors u_1 and u_2 also as shown in Fig. 12. These unit vectors do not now represent just a simple rotation of the E_x, E_y axes, but also the reflection of one of them. The negative value of Ψ_p given by Equations 35 and 36 has been cast by the SVD analysis as a positive singular value in the second matrix in Equation 71. To compensate for this convention, the direction of one of the axes (originating as the direction of an eigenvector of $\mathbf{U}$ in Equation 29) has been reversed. Any model of distortion rotating the electric fields is thus contravened. An extra physical phenomenon is required to explain the reflection of one of the rotated electric field axes. Pending such an explanation, a negative principal value (-1.8870 in the present example) must be regarded with great caution.

In normal SVD formalism the change of sign of an eigenvector, as demonstrated in the above example, may occur with little comment. In the present case however it has had the profound effect of destroying, after rotation, the "right-handedness" of the observing axes of the MT data.

14. Conclusion

Basic 2 x 2 matrices arise commonly in linear algebra, and Mohr diagrams have wide application in displaying their properties. Complementing the usual algebraic approach, they may help the student understand especially anomalous data.

Such Mohr diagrams have proved useful in checking MT data for basic errors arising in the manipulation of time-series; in checking hypothetical examples for realistic form; and in checking for errors which are demonstrated by negative determinants.

Invariants of an observed tensor under axes rotation are evident from inspection of such Mohr diagrams. The invariants may be used as indicators of the geologic dimensionality of the tensor; they may also be useful in the inversion and interpretation of MT data. Mohr diagrams of the MT phase tensor also show invariants which measure geologic dimensionality, and indicate regional geologic strike.

Attention has been given to monitoring the singularity of an MT tensor with a condition number, as tensors which approach singularity are common. Carrying out SVD on observed data with high condition numbers can indicate a direction of surficial 2D strike, for the simple case of the surficial distortion of a regional 2D MT response. In some circumstances the 2D regional strike is found in this straightforward way.

Particularly noteworthy is the observation of a critical frequency below which an observed MT tensor becomes sufficiently ill-conditioned for the surficial strike to become evident. The example in Fig. 8 shows this behaviour to apply at frequencies below 10 Hz. That a frequency-independent model produces a frequency-dependent result in this way requires care in interpretation.

Remaining problems for which proofs would augment the subject are the evident prohibition of negative *TE* values, the evident non-observation of antiparallel radial arms, and the evident non-observation of MT tensor data with negative determinant values (corresponding to Mohr circles prohibited from enclosing their origins of axes).

15. Acknowledgements

The author thanks Peter Milligan, Chris Phillips and John Weaver for many valuable discussions over recent years on the subject matter of this chapter. Data for the NQ142 example were provided by Geoscience Australia.

16. References

Bahr, K. (1988). Interpretation of the magnetotelluric impedance tensor: regional induction and local telluric distortion, *J. Geophys.* 62: 119 – 127.

Berdichevsky, M. N. & Dmitriev, V. I. (2008). *Models and Methods of Magnetotellurics*, Springer.

Bibby, H. M., Caldwell, T. G. & Brown, C. (2005). Determinable and non-determinable parameters of galvanic distortion in magnetotellurics, *Geophys. J. Int.* 163: 915 – 930.

Caldwell, T. G., Bibby, H. M. & Brown, C. (2004). The magnetotelluric phase tensor, *Geophys. J. Int.* 158: 457 – 469.

Eggers, D. E. (1982). An eigenstate formulation of the magnetotelluric impedance tensor, *Geophysics* 47: 1204 – 1214.

Groom, R. W. & Bailey, R. C. (1989). Decomposition of magnetotelluric impedance tensors in the presence of local three-dimensional galvanic distortion, *J. Geophys. Res.* 94: 1913 – 1925.

Gubbins, D. & Herrero-Bervera, E. (eds) (2007). *Encyclopedia of Geomagnetism and Paleomagnetism*, Encyclopedia of Earth Sciences, Springer.

Hobbs, B. A. (1992). Terminology and symbols for use in studies of electromagnetic induction in the Earth, *Surv. Geophys.* 13: 489 – 515.

LaTorraca, G. A., Madden, T. R. & Korringa, J. (1986). An analysis of the magnetotelluric impedance for three-dimensional conductivity structures, *Geophysics* 51: 1819 – 1829.

Lilley, F. E. M. (1993). Magnetotelluric analysis using Mohr circles, *Geophysics* 58: 1498 – 1506.
Lilley, F. E. M. (1998). Magnetotelluric tensor decomposition: Part I, Theory for a basic procedure, *Geophysics* 63: 1885 – 1897.
Lilley, F. E. M. & Weaver, J. T. (2010). Phases greater than 90° in MT data: Analysis using dimensionality tools, *J. App. Geophys.* 70: 9 – 16.
Marti, A., Queralt, P., Jones, A. G. & Ledo, J. (2005). Improving Bahr's invariant parameters using the WAL approach, *Geophys. J. Int.* 163: 38 – 41.
Press, W. H., Teukolsky, S. A., Vetterling, W. T. & Flannery, B. P. (1989). *Numerical Recipes, The Art of Scientific Computing*, Cambridge Univ. Press.
Simpson, F. & Bahr, K. (2005). *Practical Magnetotellurics*, Cambridge Univ. Press.
Smith, J. T. (1995). Understanding telluric distortion matrices, *Geophys. J. Int.* 122: 219 – 226.
Strang, G. (2005). *Linear Algebra and its Applications, 4th Edition*, Brooks–Cole.
Stratton, J. A. (1941). *Electromagnetic Theory*, McGraw–Hill.
Szarka, L. & Menvielle, M. (1997). Analysis of rotational invariants of the magnetotelluric impedance tensor, *Geophys. J. Int.* 129: 133 – 142.
Weaver, J. T. (1994). *Mathematical Methods for Geo-electromagnetic Induction*, Wiley.
Weaver, J. T., Agarwal, A. K. & Lilley, F. E. M. (2000). Characterization of the magnetotelluric tensor in terms of its invariants, *Geophys. J. Int.* 141: 321 – 336.
Weaver, J. T., Agarwal, A. K. & Lilley, F. E. M. (2003). The relationship between the magnetotelluric tensor invariants and the phase tensor of Caldwell, Bibby and Brown, *in* J. Macnae & G. Liu (eds), *Three-Dimensional Electromagnetics III*, number 43 in *Paper*, ASEG, pp. 1 – 8.
Weaver, J. T., Agarwal, A. K. & Lilley, F. E. M. (2006). The relationship between the magnetotelluric tensor invariants and the phase tensor of Caldwell, Bibby and Brown, *Explor. Geophys.* 37: 261 – 267.
Weidelt, P. & Kaikkonen, P. (1994). Local 1-D interpretation of magnetotelluric B-polarization impedances, *Geophys. J. Int.* 117: 733 – 748.
Yee, E. & Paulson, K. V. (1987). The canonical decomposition and its relationship to other forms of magnetotelluric impedance tensor analysis, *J. Geophys.* 61: 173 – 189.
Zhang, P., Roberts, R. G. & Pedersen, L. B. (1987). Magnetotelluric strike rules, *Geophysics* 52: 267 – 278.